Δελτίο της Ελληνικής Γεωλογικής Εταιρίας, τομ. XLVII , 2013
Πρακτικά 13ου Διεθνούς Συνεδρίου, Χανιά, Σεπτ. 2013

Bulletin of the Geological Society of Greece, vol. XLVII 2013
Proceedings of the 13th International Congress, Chania, Sept. 2013

MULTISTAGE ALTERATION, MINERALIZATION AND ORE–FORMING FLUID PROPERTIES AT THE VIPER (SAPPES) AU–CU–AG–TE OREBODY, W. THRACE, GREECE

Kilias S.P.[1], Naden, J.[2], Paktsevanoglou M.[1], Giampouras M.[1], Stavropoulou A.[1], Apeiranthiti D.[1], Mitsis I.[1], Koutles Th.[3], Michael K.[4] and Christidis C.[1]

[1]National and Kapodistrian University of Athens, Faculty of Geology and Geoenvironment, Department of Economic Geology and Geochemistry, Panepistimiopolis, Zographou, 157 84, Athens, Greece

[2]British Geological Survey, Nicker Hill Keyworth, Nottingham NG12 5GG, United Kingdom

[3]Thrace Minerals S.A. 74, Papadima Str., PC 69300, Sappes, Rodopi, Greece

[4]Institute of Geology and Mineral Exploration, Regional Branch of Eastern Macedonia and Thrace, Brokoumi 30, Xanthi 67100, Greece

Abstract

The mineralogy of ore and hydrothermal alteration of the high-sulfidation enargite–Au–Ag–Te Viper (Thrace) orebody, and fluid inclusions, were studied in drillcore samples. The hydrothermal system has evolved through several stages from pre-ore advanced argillic I+vuggy silica alteration, ore-stage advanced argillic II+vuggy silica alteration and silicification that has developed to argillic alteration (sericite)+silicification through pH increase, and a return to acid conditions as crosscutting post-ore advanced argillic alteration III+silicification. Ore is characterized by early barren pyrite I corroded by: (i) enargite–Au± complex Pb–Bi–Cu sulfosalts, tellurides and selenides, coexisting with euhedral quartz, and (ii) zoned pyrite II distinguished by anomalous concentrations of Au, Cu, As, Te, Bi, Pb, Se, within vuggy quartz. High-grade gold ore is also intergrown with late breccia-cementing and vein-type epithermal-like banded quartz+ pyrite. These alteration and mineralization observations are consistent with the changing composition, water fugacity, and density of an expanding column of metal-laden magmatic vapor, combined with changes in structural permeability. Part of the enargite—Au—quartz assemblages have been probably quenched from sulfosalt melt at high—temperatures (>575 ˚ C). End product of the enargite–sulfhide–silica crystallization sequence is the formation of high-grade epithermal quartz-gold colloform-banded ore during cooling and/or dilution/mixing down to ~200 ˚ C.

Key words: *high-sulfidation, sulfosalt melt, epithermal quartz, enargite.*

Περίληψη

Η ορυκτολογική σύσταση του μεταλλεύματος και των υδροθερμικών εξαλλοιώσεων, και ρευστά εγκλείσματα, του κοιτάσματος εναργίτη—Au—Ag—Te της Οχιάς (Viper), μελετήθηκαν σε δείγματα πυρήνων γεωτρήσεων. Το υδροθερμικό σύστημα ακολούθησε μία πορεία σταδιακής εξέλιξης από προγενέστερων του μεταλλεύματος προχω-

ρημένης αργιλικής εξαλλοίωσης(ΠΑΕ) Ι και σκωριώδους πυριτίωσης, ΠΑΕ ΙΙ+σκωριώδους πυριτίωσης, και πυριτίωσης που φιλοξενούν το μετάλλευμα, προς σερικιτική εξαλλοίωση+πυριτίωση μέσω αύξησης του pH, και επιστροφής στις όξινες συνθήκες σαν μεταγενέστερων του μεταλλεύματος ΠΑΕ ΙΙΙ+πυριτίωσης. Το μετάλλευμα χαρακτηρίζεται από σιδηροπυρίτη Ι που αντικαθίσταται από: (1)εναργίτη+Au±πολυσύνθετα θειοάλατα, τελλουρίδια και σεληνήδια των Pb–Bi–Cu, που συνυπάρχει με ιδιόμορφο χαλαζία, και (2) ζωνοειδή σιδηροπυρίτη που διακρίνεται από ανώμαλες συγκεντρώσεις Au, Cu, As, Te, Bi, Pb και Se, που φιλοξενούνται από κοιλότητες σκωριώδους χαλαζία. Υψηλές περιεκτικότητες σε χρυσόχαρακτηρίζουν επίσης τον ύστερο ταινιωτό χαλαζία+σιδηροπυρίτη επιθερμικού τύπου. Αυτές οι παρατηρήσεις συμφωνούν με μεταβολές χημικής σύστασης, πτητικότητας του νερού και πυκνότητας μίας στήλης επεκτεινόμενου μαγματικού ρευστού με υψηλό μεταλλικό δυναμικ, σε συνδυασμό με την περατότητα λόγω τεκτονισμού. Τα συσσωματώματα εναργίτη-Au-χαλαζία πιθανώς αποχωρίστηκαν, τουλάχιστον τμηματικά, από ένα θειούχο τήγμα σε υψηλές θερμοκρασίες (>575°C).Η πορεία κρυστάλλωσης εναργίτη-σουλφιδίων-χαλαζία, κατά τη διάρκεια της επέκτασης του μαγματικού ρευστού, έχει σαν τελικό παράγωγο την απόθεση χρυσοφόρου μεταλλεύματος που συνδέεται με επιθερμικό χαλαζία λόγω ψύξης και/ή αραίω-σης/ανάμειξης έως ~200°C
Λέξεις κλειδιά: *υψηλή σουλφιδίωση, σιδηροπυρίτης, εναργίτης, χημική ζώνωση*.

1. Introduction

The Viper orebody of the Sappes Gold Project (SGP), Sappes, Thrace–NE Greece (Figure 1), is a volcanic-hosted high-grade Au–Cu–Ag deposit that has a measured resource of 710 kt @ 22.2 g/t Au; 11.5 g/t Ag; 0.4 % Cu, and inferred resource of 1,109 kt@17.2 g/t Au; 8.8 g/t Ag; 0.3% Cu (Glory Re-sources, 2012). The economic mineralization at Viper forms a NW-trending, elongated, blind, flat-lying ~60 m thick orebody, and has estimated dimensions of 550 by 1310 m, at a depth of approximately 200–240 m below the current surface. Ore occurs as hydrothermally altered, multi-stage breccias, and disseminations in stockwork quartz-veinlets and vug-fillings. The SGP also comprises outcropping epithermal-style Au- and Te-rich mineralization at St Demetrios (<200 m from Viper) and St Barbara (2.5 km to south of Viper), plus a Cu-rich porphyry-style prospects at Koryfes Hill, (Michael, 2004; Voudouris, 2006; Voudouris et al., 2006). Porphyry and epithermal mineralization in the area has been dated at about 32 Ma (Ortelli et al., 2009). In this paper we present the first data derived from the Viper orebody and utilize hydrothermal alteration patterns, ore mineralization textures and fluid inclusion microthermometry to decipher its genesis.

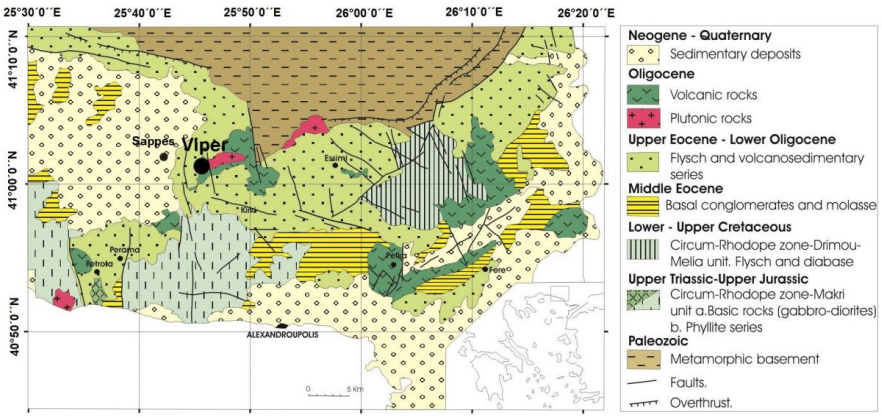

Figure 1 - Simplified geology of Western Thrace showing the location of Viper deposit (modified after Papadopoulos, 1982).

2. Geology and Mineralization

The geological structure of western Thrace consists of three units (Figure 1): a) Palaeozoic or older metamorphic basement (Marchev et al., 2005), b) the Jurassic to early Creataceous age Circum Rhodope Belt (Makri Unit) (Papadopoulos, 1982) and c) Late Eocene to Oligocene sedimentary and volcanosedimentary rocks and Oligocene–Miocene plutonic, subvolcanic and volcanic rocks (Voudouris et al., 2006). In the Sappes area (Figure 1), the Viper deposit is spatially associated with an Oligocene to Lower Miocene composite calc-alkaline to high-K calc-alkaline volcanic rocks (Figure 1), which in turn is linked to Middle to Upper Eocene volcaniclastic sedimentary sequences that discordantly overlying the Mesozoic Circum Rhodope metamorphic basement (Papadopoulos, 1982; Michael et al., 1995; Arikas and Voudouris, 1998; Michael, 2004; Voudouris et al., 2006; Voudouris, 2006). The volcanic rocks comprise a suite of calc-alkaline to high-K calc-alkaline andesites–dacites and dacite and rhyolite porphyries (Voudouris et al., 2006), and hydrothermally altered polymictic and mixed monomictic to polymictic volcanic breccias. Host rocks are dacitic–andesitic polymictic breccia units, and locally mixed monomictic to polymictic volcanic breccias. Bodies of equigranular to porphyritic mineralized microdiorite (Koryfes Hill) and quartz monzodiorite (~32 Ma, Voudouris, 2006) occur as small irregular stocks in the Sappes area. Later (<27 Ma, Voudouris, 2006) dacite and rhyolite porphyry dikes intruded the monzodioritic/dioritic rocks along N to NW regional fault zones. Surface expressions of porphyry-style (Koryfes Hill) and Te-rich epithermal style (St Demetrios, St. Barbara) mineralization have been reported in the Sappes area (Voudouris et al., 2006).

3. Materials and Methods

Samples were collected from drill core. The mineralogy of the ore and alteration assemblages was evaluated in the laboratories of the Department of Economic Geology and Geochemistry, Athens University, by polished thin section transmitted and reflected light petrography, powder X-ray diffraction (PXRD), scanning electron microscopy (SEM), and energy-dispersion spectrometry (EDS). Powder X-ray diffraction [Bruker Model D5005, CuKa radiation at 40kV and 40mA, using a 0.02° step size and 1 or 2 second per step counting time, graphite monochromator], was conducted on randomly oriented samples. The <2 μm fractions were separated by settling, dried on Si-wafers at room temperature and then were solvated with ethylene-glycol vapour at 65°C overnight for maximum saturation. Fluid inclusion microthermometry was undertaken on doubly polished plates (each ~0.15 mm thick), using a LINKAM THSM600 heating-freezing stage, also at Athens University. Calibrations were carried out using commercially available standards. The precision of measured temperatures is ±1.0° and ±0.3°C for heating and freezing, respectively.

4. Results

4.1. Hydrothermal Alteration

The superposition of at least 3 stages of hydrothermal alteration and mineralisation, which are strongly correlated with hydrothermal breccias and veinlets, namely pre-ore, ore and post-ore stages, have been identified.

4.1.1. Pre-Ore Stage I

Vuggy silica alteration: Vuggy silica I contains fine-grained (up to 0.5mm) jigsaw quartz. Vugs, which account for ~10 percent of the rock, have variable size and are commonly lined by chalcedonic quartz. *Advanced argillic alteration I*: Dominates the top of the preserved hydrothermal system above the Viper orebody. The alteration assemblage is quartz, pyrite, diaspore and pyrophyllite. Upward grading leads to alunite±dickite, kaolinite, fine grained pyrite and microcrystalline jigsaw quartz.

4.1.2. Ore-Stage IIa

Vuggy silica alteration: Vuggy silica consists of fine to medium-grained (500µm to 3mm) jigsaw quartz with serrated margins (Figure 2A). Cavities are sometimes filled by cockade quartz, with successive narrow and subparallel bands of crustiform quartz. *Advanced argillic alteration II:* This alteration (Figure 2B) is characterized by vug-filling clusters of coarse-grained minerals comprising assemblages of dickite/kaolinite–quartz–pyrite–aluminium-phosphate-sulfate minerals of the alunite supergroup (APS). Alunite grains are tabular to bladed and overgrown by the APS minerals woodhouseite, svanbergite and hinsdalite (Figure 2C). Dickite occurs as fine-grained masses intergrown with very fine grained quartz and alunite (Figure 2B).

4.1.3. Ore-stage IIb

Argillic (sericitic) alteration: Sericite occurs as rosettes in vugs within colloform quartz veinlets (Figure 2D). In addition, fine-grained flaky clusters of sericite enclose diaspore formed during pre-ore stage I advanced argillic alteration (Figure 2E). Sericite has also been observed by in sharp contact with dickite (Figure 2F). Crosscutting relationships and replacement textures constrain the timing of this alteration to postdate pre-ore advanced argillic alteration I. *Silicification:* This alteration is widespread and its principle feature is the development of colloform-banded quartz, exhibiting combined spherical, botryoidal, reniform and mammillary forms (Figure 2G,H) Silicification occurs along fractures, as vug fills and breccia cements).

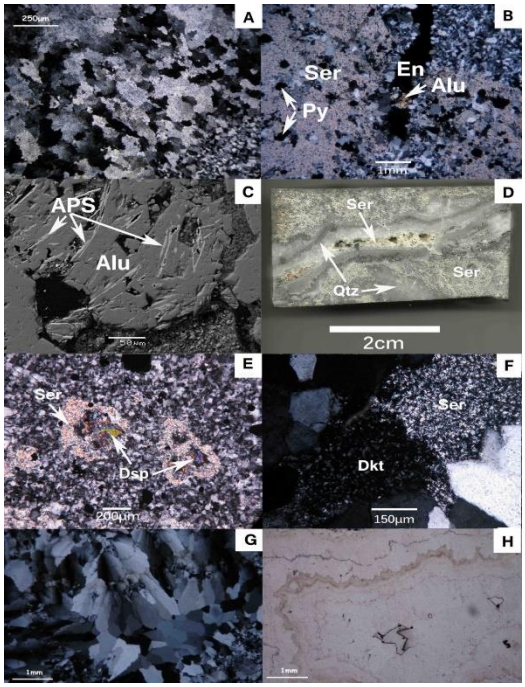

Figure 2 - Photomicrographs and a BSE image of the ore-stage hydrothermal alteration assemblages and textures. A. Vuggy silica consisting of medium-to fine-grained jigsaw quartz with serrated margins. Crossed polars. B. Elongated vug filled with advanced argillic alteration assemblages of tabular alunite crystals, enargite, mantled by microcrystalline jigsaw quartz, pyrite and sericite patches (argillic alteration). Crossed polars. C. 8Tabular alunite grains containing Sr-APS minerals (svanbergite). D. Colloform-banded quartz veinlet with sericite rossetes in vugs crosscutting argillic assemblage of patchy sericite+quartz. E. Diaspore crystals enclosed in flaky sericite patches. F Sericite in sharp contact with dickite. G. Colloform banded jigsaw/plumose quartz. H. Same as G in plain polarized light. Ser:Sericite, Py:Pyrite, Dck:Dickite, Alu:Alunite, Dsp:Diaspore, Qtz:Quartz.

4.1.4. Post-ore stage III

Advanced argillic alteration III: Generally, stage III advanced argillic alteration is restricted to quartz–alunite–pyrite containing veins, veinlets and cavity fillings that crosscut all previous alteration stages. Two varieties of alunite have been recognised: a) euhedral bladed and irregular coarse- to medium-grained needle-like crystals and b) pseudocubic alunite crystals. Dickite/kaolinite occurs as either dark extremely fine-grained masses or medium-grained clusters with recognizable flakes. *Silicification* Vug-filling amethystine quartz and barite represent the final alteration system of the Viper hydrothermal system. Barite crystals are frequently corroded and their size is variable. Amethystine quartz has plumose or jigsaw texture and is distinguished by a gradual increase of the grain size from the margins to the center of cavities.

4.2. Enargite-Gold and Gold Ore Mineralization

Ore mineralogy at Viper is dominated by sulfosalt–sulfide–Au assemblages intimately associated with ore-stage II hydrothermal alteration. It is hosted by vuggy silica and Au-bearing pyrite in colloform-banded quartz II. Ore is characterized by early barren pyrite I followed and replaced by: (i) enargite±chalcopyrite±galena±Au±complex Pb–Bi–Cu sulfosalts, tellurides and selenides (Figure 3A,B,C) and, (ii) zoned pyrite II which is distinguished by anomalous concentrations of Au, Ag, Cu, As, Te, Bi, Pb and Se (Figure 3D). Moreover, high-grade gold ore with pyrite, in which enargite is absent, is intergrown with Stage IIb colloform-banded quartz (Figure 3E). The deepest high-grade samples (~350 m) along discovery drillhole DV36 contain vapor-rich inclusion laden euhedral quartz I crystals within enargite that corrodes earlier pyrite I. Pyrite I is subhedral to anhedral, fractured, infilled, and strongly corroded. It generally has a porous texture, perhaps due to leaching. Enargite textures contain distinct domains of symplectic enargite−chalcopyrite intergrowths similar to those observed in quenched experimental sulfide melts (Figure 3F). Rarely, pyrite II crystals are mantled by pyrite I. Pyrite II contains three types of growth zones: (1) As-rich zones that are enriched in Cu±Bi±Sb±Te±Se±Pb─bearing sulfide/sulfosalt mineral inclusions (Figure 4), (2) As- poor, inclusion-free, zones with significantly lower or absent concentrations of these elements (Figure 4) and, (3) growth zones outlined by micro-vugs that locally host native gold grains (Figure 3D). Micron-sized gold at Viper occurs as: (i) inclusions of native gold in pyrite I, (ii) native gold intergrown with enargite, alunite and APS minerals (Figure 3B), or as vug infillings associated with complex Pb–Bi–Cu sulfosalts, tellurides and selenides, and rarely sphalerite, (iii) native gold decorating "vuggy" growth zones in pyrite II (Figure 3D), and (iv) intergrown with epithermal (*sensu stricto*, Bodnar et al., 1985) colloform-banded quartz II (Figure 3E), and (v) sub-micron to micron-sized inclusions or chemically held gold within, pyrite II and enargite (*unpublished data*). Native gold may contain up to 9 wt% Ag.

4.2. Fluid Inclusion Data

4.2.1. Samples and Methodology

Analyses of primary fluid inclusions focused on ore-stage IIb and post-ore stage III euhedral epithermal quartz II (*sensu stricto*; Bodnar et al., 1985). Twenty-five (25) doubly polished thick sections (~150 μm thick) and chips sampled with the use of a microcorer sampler, were prepared from eighty-five (85) drillcore high-grade (11–63.4 g/t) intersection samples; the samples are from the discovery boreholes DV36A, DV42 and SD8, and cover about 90 m, 10 m and 3 m of drillcore, respectively. Salinities have not been corrected for the potential of dissolved CO_2 on freezing point depression.

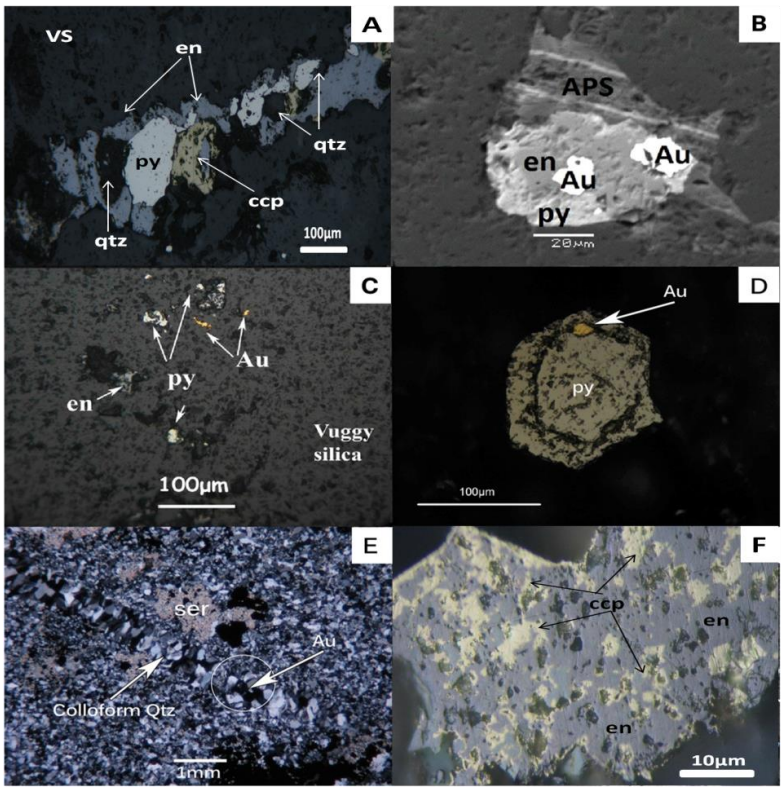

Figure 3 - A. Dissolution of early pyrite I by enargite (En) and chalcopyrite (Ccp) with euhedral quartz (Qz) infilling void spaces within "vuggy" silica. B. BSE image of native gold intergrown with enargite,alunite and APS minerals, showing Ca-Sr-Pb-rich bands, in vug. C. Vuggy quartz infilling by native gold, enargite and pyrite I. D. Native gold on a pyrite II growth zone E. Native gold intergrown with colloform-banded quartz crosscutting argillic alteration. F. Symplectic enargite-chalcopyrite intergrowths resembling quenched experimental sulfide melts (en: enargite, py: pyrite, ccp: chalcopyrite, qtz: quartz, VS: vuggy silica, Au: gold, APS: aluminum-phosphate-sulfate minerals, ser: sericite).

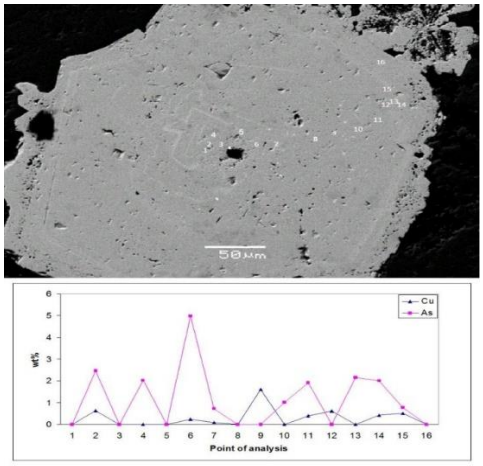

Figure 4 - Top: BSE image of a coarse-grained, trace element-rich ore-stage zoned pyrite II, showing oscillatory zoning: 'bright' zones in BSE are enriched with As and/or Cu. Bottom: Element profile across the pyrite grain in "top". Points of analysis refer to numbers in "top".

4.2.2. Fluid Inclusion Types

Two types of primary fluid inclusions were identified: Type 1 includes two-phase, liquid-rich (10−45% vapor) fluid inclusions, and Type 2 fluid inclusions are vapor-rich (>80% vapor), two phase inclusions. Primary inclusions occur as isolated, randomly distributed inclusions, or in crystal growth zones. The majority of measured inclusions ranged between 20μm and 30μm. Inclusion shapes are variable including rounded, angular and equant or negative crystal shapes. Fluid inclusion assemblages (FIA's) defined by coexisting, type 1 and 2 inclusions were observed in quartz throughout the drillcore depth range studied. Type 1 inclusions with consistent liquid-to-vapor ratios decorate growth zones of post-ore stage III quartz. We did observe single-phase, liquid-filled inclusions coexisting with vapor-filled inclusions in ore-stage IIb samples, which suggest that vapor-rich inclusions were formed by vapor-phase trapping rather than necking (Bodnar et al., 1985). Liquid CO_2 or CH_4 were not observed or detected during freezing runs.

4.2.3. Microthermometry

Data were obtained only from type 1 inclusions, because phase changes in type 2 inclusions proved difficult to observe and accurately record. Microthermometric measurements of Type 1 inclusions show liquid Th that range from 140°C to 270°C and $T_{m\text{-}ice}$ between –0.9 and –3.3°C, corresponding to salinities between 1 and 6 wt% NaCl equiv, which fall within typical ranges for this variety of epithermal gold deposit (e.g. Simmons et al., 2005) (Figure 7). First melting temperatures range from –20.4 to –34.1°C and are consistent with H_2O–NaCl (±KCl±$MgCl_2$) salt solutions (Bodnar et al., 1985). Microthermometric data show trends of decreasing T_h and salinity from the ore-stage IIb quartz to the post-ore stage III quartz.

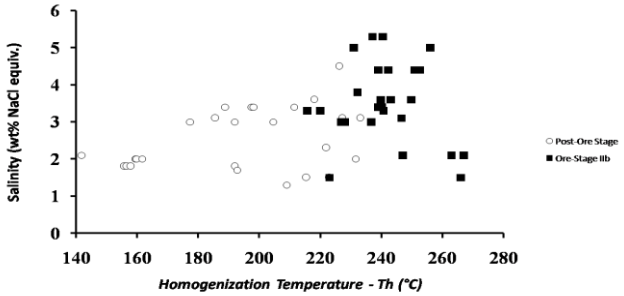

Figure 5 - Th-salinity diagram showing the evolution of hydrothermal fluids at Viper deposit. The trend is consistent with mixing and/or boiling.

5. Discussion – Concluding Remarks

The Viper Au–Ag–Cu–Te orebody is one of several Tertiary volcanic-hosted precious and base metal Te-rich deposits on the margins of the eastern Greek Rhodope, which are considered to reflect formation in a porphyry−epithermal environment (Voudouris 2006; 2010, Voudouris et al., 2011). While alike in many features to typical high-sulfidation epithermal deposits (e.g. Hedenquist et al., 2000; Simmons et al., 2005), Viper differs from other deposits of this type most notably because it is characterized by multistage evolution involving early magmatic and later epitherma" (*sensu stricto*; Bodnar et al., 1985) ore stages.

5.1. Multistage Hydrothermal System

High-sulfidation gold deposits are commonly characterized by a pre-sulfide vuggy residual quartz−alunite±pyrophyllite advanced alteration envelope, and a subsequent contrasting sequence of ore-stage sulfide assemblages typically including pyrite, that progresses through a range of

sulfosalt minerals (i.e. enargite and tennantite), to later sulfosalt, sulfide and telluride minerals, Au, nd Ag; this progression is tightly constrained by syn-hydrothermal brittle faulting and/or brecciation (Berger and Henley, 2011; Henley and Berger 2011). The mineral relationships shown in Figures 2 and 3 illustrate a complex rapidly evolving sulfate–sulfide–sulfosalt–silica depositional setting at Viper, and the apparent superposition of recurring events of advanced argillic alteration. The earliest stage (Stage I), which is unrelated to the ore, involved pervasive quartz+alunite+pyrite±dickite/kaolinite that graded downwards to pyrophyllite–quartz–pyrite±diaspore. This, when combined with associated sulfosalt-sulfide free vuggy quartz textures, is strongly indicative of early extremely acid (pH<2) fluids (Stoffregen, 1987). A second stage of advanced argillic alteration (dickite−quartz−pyrite−APS minerals−alunite) (Stage IIa), followed by a stage of argillic alteration (quartz−sericite) (Stage IIb) which in turn was suceeded by colloform-banded quartz, indicate that pH temporarily evolved to higher values (~ 6), as a result of dilution, **or** the interaction of the fluid with the rock at progressively lower fluid/rock ratios and decreasing temperature (Chouinard et al., 2005; Scher et al., 2013). A third stage of vein-type crosscutting advanced argillic alteration (quartz–alunite–pyrite) (Stage III) indicates a return to acidic conditions. Late-stage silicification (quartz–barite) (Stage III) characterized by amethystine quartz and barite mark the waning stages of the hydrothermal activity.

5.2. Ore Forming Processes A: the Magmatic Connection

In the light of: (i) euhedral quartz crystals wholly enclosed within veinlets and cavities with enargite that dissolves early pyrite I (Figure 3A,B), (ii) asymmetrical zonation of arsenic (±Cu, Te, Sb) in pyrite II around earlier leached pyrite±quartz (Figure 4), and, (iii) symplectic enargite−chalcopyrite textures that resemble quenched melts (e.g. Tomkins, 2010) (Figure 3F), (iv) vapor-rich fluid inclusions in quartz within enargite, we suggest that sulfosalt crystallization within vugs and veinlets from a composite vapor−saturated Fe-Cu-As-Sb-S (±Si, P, Pb, Ca, Te, Au, Ag, Se, Bi) sulfosalt melt at high temperatures; the perfect hexagonal morphology of quartz crystals in our samples suggests, but does not prove deposition temperatures in the β-quartz field (>575°C) (Mavrogenes et al., 2010; Henley and Berger, 2011; Henley et al., 2012). Furthermore, the pyrite to enargite reaction characterizes high-sulfidation lode copper–gold deposits worldwide (i.e. El Indio [Chile], Lepanto [Philippines], Summitville [USA], Red Mountain [USA]; Berger and Henley 2011), and may suggest sulfide-sulfate deposition via solidification of a sulfosalt melt that condensed from an expanding magmatic vapor phase at high-temperatures (>600°C) and near lithostatic pressures, in a non-equilibrium chemical environment, following higher temperature deposition of crystalline pyrite. Our data support such a model for the formation of least part of the enargite and pyrite II–gold (±Ag±Sb±Pb±Te±Se) mineralization at Viper. A vapor rich environment at Viper is also supported by the abundance of vapor-rich inclusions in lower-temperature auriferous "epithermal" quartz (*sensu stricto*; Bodnar et al., 1985), and confirms a wide range of temperatures and temperature gradients during development of the ore. The involvement of magmatic vapor is further supported by oscillatory zonation patterns in pyrite II adjacent to pyrite I and quartz I contacts (Deditius, 2009; Mavrogenes et al., 2010).

5.3. Ore-forming Processes B: the Epithermal Connection

Temperature–pressure profiling for HS gold deposits is burdened with problems (Berger & Henley 2011; Henley& Berger 2011). This is because, the characteristic silica−alunite assemblages of HS environments preserve local domains developed during cooling and recrystallization in the presence of acid condensate and groundwater, so that fluid inclusion data from crystalline quartz record only cooling history rather than primary events (Henley and Berger, 2012). Unlike most HS gold deposits, auriferous colloform−banded jigsaw, plumose, and crustiform quartz is ubiquitous throughout the Viper orebody (Figure 3E). Our fluid inclusion data stemming from this epithermal quartz indicate boiling of a low-salinity fluid during ore-stage IIb breccia formation because: (i) vapor- and liquid-rich inclusions coexist in boiling fluid inclusion assemblages (ii) decreasing T_h and salinity trends possibly the result of boiling (e.g. Bodnar et al., 1985) (Figure 5); boiling in

this case would result in competing effects of increased salinity, and decreased apparent salinity due to CO_2 degassing in the residual fluid (Hedenquist and Henley, 1985), (iii) gangue silica textural evidence for colloform-banded quartz (Figure 2G,H) indicating rapid temperature/pressure drop that leads to oversaturation and rapid deposition, such as might occur during boiling (Bodnar et al., 1985). Conversely, the trend shown in figure 5 could be the result of mixing of low (~0–2 wt % NaCl equiv) and moderate-salinity (~10 wt% NaCl equiv) fluids (Hedenquist and Henley, 1985). At Viper, fluid inclusion data (Figure 5) indicate that formation temperature was higher in the epithermal ore-stage IIb quartz (270–220°C), and decreased through the post-ore stage III quartz from ~230–160°C.

5.4. Environment and Conditions of Ore Deposition

We interpret enargite–Au–Ag–Te ore deposition at Viper to have occurred by two main processes that contributed to the high-grade and complex nature of the deposit. First, solidification of a Fe–Cu–As–Sb–S (±Pb, Zn, Si, P, Ca, Sr, Te, Se, Au, Ag, Bi) sulfosalt melt condensed from an expanding magmatic vapor phase at high temperatures (>575°C) and near lithostatic pressures (Mavrogenes et al., 2010; Henley and Berger, 2011). Second, boiling and/or mixing, and mixing-induced cooling, which is most effective at depositing quartz (Simmons et al., 2005), produced the ubiquitous auriferous silica phase at Viper. This epithermal quartz-flooding may represent the end-product of the sulfosalt−sulfide crystallization sequence within an expanding plume of magmatic vapor, the spatial control of which has been effected by active fracturing and brecciation (Henley and Berger, 2011). The epithermal silica at Viper is highly probably recrystallized and homogenization temperatures data record trapping and gold–quartz II deposition during cooling from >500°C the primary deposition temperature of the quartz I and enargite−gold assemblage (Mavrogenes et al., 2010; Henley and Berger, 2011), through stage II temperatures of 270–220°C, to the waning stages of post-ore assemblages at 230–160°C. Thus, the Viper orebody was formed by evolving magmatic to hydrothermal−epithermal processes that took place in multistage sequences of advanced argillic, vuggy silica, and argillic alteration and silicification, either earlier than, contemporaneous with or later than ore. The complexity of the Viper system is a cumulative consequence of the chemical evolution within an expanding column of ore-forming magmatic vapor, in combination with changes in structural permeability (i.e. multistage hydrothermal brecciation) due to the coupling of alteration and fracture dynamics (Henley and Berger, 2011; Berger and Henley, 2011).

6. Acknowledgments

Funding by the Special Account for Research Grants of the National and Kapodistrian University of Athens to SPK is gratefully acknowledged. JN publishes with the permission of the Director of the British Geological Survey.

7. References

Arikas K. and Voudouris P. 1998. Hydrothermal alterations and mineralizations of magmatic rocks in the southern Rhodope Massif, *Acta Vulcanol*, 10, 353–365.

Berger B.R. and Henley R.W. 2011. Magmatic-vapor expansion and the formation of high-sulfidation gold deposits: Structural controls on hydrothermal alteration and ore mineralization, *Ore Geology Reviews*, 39(1), 75-90.

Bodnar R.J., Reynolds T.J. and Kuehn C.A. 1985. Fluid-inclusion systematics in epithermal systems, *Reviews in Economic Geology*, 2, 73−97.

Chouinard A., Williams-Jones A. E., Leonardson R.W., Hodgson C.J., Silva P., Téllez C. and Rojas F. 2005. Geology and genesis of the multistage high-sulfidation epithermal Pascua Au-Ag-Cu deposit, Chile and Argentina, *Economic Geology*, 100(3), 463-490.

Deditius A., Utsunomiya S., Ewing R., Chryssoulis S., Venter D. and Kesler S. 2009. Decoupled geochemical behavior of As and Cu in hydrothermal systems, *Geological Society of America*, 37, 707-710.

Glory Resources 2012 website (http://www.gloryresources.com.au/projects/sapes-gold-project/)

Hedenquist J. W. and Henley R. W. 1985. The importance of CO 2 on freezing point measurements of fluid inclusions; evidence from active geothermal systems and implications for epithermal ore deposition, *Economic geology*, 80(5), 1379-1406.

Henley R. W. and Berger B.R. 2011. Magmatic-vapor expansion and the formation of high-sulfidation gold deposits: Chemical controls on alteration and mineralization, *Ore Geology Reviews*, *39*(1), 63-74.

Henley R. W. and Berger B.R. 2012. Pyrite–sulfosalt reactions and semimetal fractionation in the Chinkuashih, Taiwan, copper–gold deposit: a 1 Ma paleo-fumarole, *Geofluids*, *12*(3), 245-260.

Henley R. W., Mavrogenes J. and Tanner D. (2012). Sulfosalt melts and heavy metal (As-Sb-Bi-Sn-Pb-Tl) fractionation during volcanic gas expansion: the El Indio (Chile) paleo-fumarole, *Geofluids*, *12*(3), 199-215.

Marchev P., Kaiser-Rohrmeier M., Heinrich C., Ovtcharova M., von Quadt A. and Raicheva R. 2005. Hydrothermal ore deposits related to post-orogenic extensional magmatism and core complex formation: The Rhodope Massif of Bulgaria and Greece, *Ore Geology Reviews*, 27, 53-89

Mavrogenes J., Henley R. W., Reyes A. G. and Berger B. 2010. Sulfosalt melts: Evidence of high-temperature vapor transport of metals in the formation of high-sulfidation lode gold deposits, *Economic Geology*, 105(2), 257-262.

Michael C., Perdikatsis V., Dimou E. and Marantos I. 1995. Hydrothermal alteration and ore deposition in epithermal precious metal deposit of Agios Demetrios, Konos area, Northern Greece, *Bull. Geol. Soc. Greece*, sp. Publ., 4/2, 778-782.

Michael C. 2004. Epithermal systems and gold mineralization in western Thrace (North Greece), *Bull. Geol. Soc. Greece*, 36, 416-423.

Ortelli M., Moritz R., Voudouris P. and Spangenberg J. 2009. Tertiary porphyry and epithermal association of the Sapes-Kassiteres district, Eastern Rhodopes, Greece, In*: Proceedings of the 10th biennial SGA meeting*, Townsville, Australia, August 2009, Williams, P. et al (eds), 536-538.

Papadopoulos P. 1982. Geological Map of Greece, *Maronia sheet*, scale 1:50000, I.G.M.E., Athens.

Ring U., Glodny J., Will T. and Thomson S., 2010. The Hellenic Subduction System: High-Pressure Metamorphism, Exhumation, Normal Faulting, and Large-Scale Extension, *Annual Review of Earth and Planetary Sciences*, 38, 45-76.

Scher S., Williams-Jones A. E. and Williams-Jones G. 2013. Fumarolic Activity, Acid-Sulfate Alteration, and High Sulfidation Epithermal Precious Metal Mineralization in the Crater of Kawah Ijen Volcano, Java, Indonesia, *Economic Geology*, 108(5), 1099-1118.

Simmons S. F., White N. C. and John D. A. 2005. Geological characteristics of epithermal precious and base metal deposits, *Economic Geology*, 100th Anniversary Volume, 485-522.

Tomkins A. G. 2010. Wetting facilitates late-stage segregation of precious metal–enriched sulfosalt melt in magmatic sulfide systems, *Geology*, 38(10), 951-954.

Voudouris P. 2006. A comparative mineralogical study of Te-rich magmatic-hydrothermal systems in northeastern Greece, *Mineralogy and Petrology*, 87, 241-275.

Voudouris P., Tarkian M. and Arikas K. 2006. Mineralogy of telluride-bearing epithermal ores in the Kassiteres-Sappes area, western Thrace, Greece, *Mineralogy and Petrology*, *87*(1-2), 31-52.

Voudouris P. C. 2011. Conditions of formation of the Mavrokoryfi high-sulfidation epithermal Cu–Ag–Au–Te mineralization (Petrota Graben, NE Greece), *Mineralogy and Petrology*, *101*(1-2), 97-113.